Revision 3

The system Na_2CO_3-$FeCO_3$ at 6 GPa and its relation to the system Na_2CO_3-$FeCO_3$-$MgCO_3$

Anton Shatskiy[1,2*], Sergey V. Rashchenko[1,2], Eiji Ohtani[1,3], Konstantin D. Litasov[1,2], Mikhail V. Khlestov[1], Yuri M. Borzdov[1,2], Igor N. Kupriyanov[1,2], Igor S. Sharygin[1,2], Yuri N. Palyanov[1,2].

[1]V.S. Sobolev Institute of Geology and Mineralogy, Russian Academy of Science, Siberian Branch, Koptyuga pr. 3, Novosibirsk 630090, Russia

[2]Novosibirsk State University, Novosibirsk 630090, Russia

[3]Department of Earth and Planetary Material Science, Tohoku University, Sendai 980-8578, Japan

Abstract

The phase relations in the Na_2CO_3-$(Fe_{0.87}Mn_{0.06}Mg_{0.07})CO_3$ system have been studied in Kawai-type multianvil experiments using graphite capsules at 6.0 GPa and 900-1400 °C. Subsolidus assemblages comprise the stability fields of $Na_2CO_3 + Na_2Fe(CO_3)_2$ and $Na_2Fe(CO_3)_2$ + siderite with the transition boundary at $X(Na_2CO_3)$ = 50 mol%. Intermediate $Na_2Fe(CO_3)_2$ compound has rhombohedral $R\bar{3}$ eitelite structure with cell parameters a = 4.9712(16) Å, c = 16.569(4) Å, V = 354.61(22). The Na_2CO_3-$Na_2Fe(CO_3)_2$ eutectic is established at 1000 ºC and 66 mol% Na_2CO_3. $Na_2Fe(CO_3)_2$ disappears between 1000 and 1100 ºC via incongruent melting to siderite

and a liquid composed of about 55 mol% Na_2CO_3 and 45 mol% siderite. Siderite remains a subliquidus phase at 1400 ºC at $X(Na_2CO_3) \leq 30$ mol%.

The ternary Na_2CO_3-$FeCO_3$-$MgCO_3$ system can be built up from the corresponding binary systems: two systems with intermediate $Na_2(Mg,Fe)(CO_3)_2$ phase, which melts congruently at the Mg-rich side and incongruently at the Fe-rich side, and the $(Mg,Fe)CO_3$ system with complete solid solution. The phase relations suggest that the maximum contribution of $FeCO_3$ component into the lowering solidus temperatures of Na-bearing carbonated mantle domains could not exceed several tens °C.

1. Introduction

Previous experimental studies demonstrate that siderite forms a complete solid solution with magnesite, which would be stable under upper and lower mantle conditions and may transport carbon in subducting lithospheric plates into the deep mantle (Dasgupta et al., 2004; Santillán and Williams, 2004; Lavina et al., 2010; Boulard et al., 2011; Franzolin et al., 2011; Litasov et al., 2013a). The observations of $FeCO_3$ as inclusions in diamond in association with the $(Mg,Fe)SiO_3$ + $(Mg,Fe)O$ assemblage (Stachel et al., 2000) supports these experimental observations. Yet, in the presence of alkalis, carbonates could melt at much lower temperatures to form alkali-rich carbonatite melts (Brey et al., 2011; Grassi and Schmidt, 2011; Litasov et al., 2013c). Such melts were also found as recrystallized microinclusions in diamonds from kimberlites (Navon, 1991; Schrauder and Navon, 1994; Zedgenizov et al., 2007; Weiss et al., 2009). Owing to their low density (Genge et al., 1995; Guillot and Sator, 2011), enhanced wetting properties (Hunter and McKenzie, 1989; Minarik and Watson, 1995; Yoshino et al.,

2010), and ability to transport silicate components (Shatskiy et al., 2013b), such melts could stem from subducted oceanic lithosphere and percolate upwards along grain boundaries (Hammouda and Laporte, 2000) or by means of diapiric ascent (Litasov et al., 2013b; Litasov et al., 2013c). This could suppress the amount of carbon, which can be potentially transported down to the transition zone and lower mantle (Dasgupta and Hirschmann, 2010). It is, therefore, essential to know phase relations in simple alkali-alkaline earth and Fe-bearing carbonate systems under mantle conditions.

Although phase relations in the alkali-earth carbonate systems were studied extensively from upper down to lower mantle conditions, e.g., (Katsura and Ito, 1990; Ono et al., 2007; Nagai et al., 2010; Franzolin et al., 2011; Boulard et al., 2012), the studies of the alkali-bearing carbonate systems were limited to Fe-free compositions (Eitel and Skaliks, 1929; Cooper et al., 1975; Shatskiy et al., 2013a; Shatskiy et al., 2013c; Shatskiy et al., 2013d). At the same time, an investigation of Fe-bearing carbonate systems, e.g. Na_2CO_3-$FeCO_3$-$MgCO_3$-$CaCO_3$, has particular importance, given the abundance of Na and Fe in carbonatite melt inclusions in diamonds (up to 7-14 wt% Na_2O and 11-58 wt% FeO) from the upper (Tomlinson et al., 2006; Klein-BenDavid et al., 2009; Zedgenizov et al., 2009) and lower mantle (Kaminsky et al., 2009b; Kaminsky et al., 2013) as well as the abundance of Fe-bearing species in hydrothermally altered oceanic crust subducted into the Earth's mantle (Lecuyer and Ricard, 1999). As a part of an investigation of the Na_2CO_3-$FeCO_3$-$MgCO_3$-$CaCO_3$ system, the corresponding binary systems have to be examined. Since phase relations in the Na_2CO_3-$MgCO_3$, Na_2CO_3-$CaCO_3$, $FeCO_3$-$MgCO_3$, $CaCO_3$-$MgCO_3$ and $CaCO_3$-$FeCO_3$ systems at 6 GPa have been already studied (Buob et al., 2006; Shatskiy et al., 2013a; Shatskiy et al., 2013d; Shatskiy

et al., 2014a), here we present new experimental data on phase relations in the Na_2CO_3-siderite system at 6 GPa and 900-1700 ºC. Using obtained data we discuss a possible topology of the ternary Na_2CO_3-$FeCO_3$-$MgCO_3$ system and the influence of iron component on melting in the petrologically important system Na_2CO_3-$CaCO_3$-$MgCO_3$.

2. Experimental methods

Experiments were conducted using Kawai-type multianvil apparatuses at Tohoku University (Sendai, Japan) (Shatskiy et al., 2011). We employed ZrO_2 pressure media with edge length of 20.5 mm and WC anvils with truncation edge length of 12 mm. Sample heating was achieved using a graphite heater, 4.5/4.0 mm in outer/inner diameter and 11 mm in length. Temperature was controlled using WRe(3%/25%) thermocouple inserted into the heater center via walls and electrically insulated by Al_2O_3 tubes. The cell configuration and calibration procedures were described in details by Shatskiy et al. (2013c). In this study we used siderite from Bakal deposit, South Ural, Chelyabinsk region, Russia. Siderite crystals were ground and sintered to homogeneous sample at 6 GPa and 900 °C. Based on EDS and WDS analysis the composition of recovered siderite corresponds to $(Fe_{0.87}Mn_{0.06}Mg_{0.07})CO_3$. Then this siderite was milled and mixed with synthetic Na_2CO_3 in agate mortar under acetone and loaded into graphite cassettes (multicharged sample holders). The cell assembly contained four cassettes. In turn, each cassette contained four holes, 0.9 mm in diameter. To study the present system we used two lower cassettes (i.e., eight holes with different sample compositions shown in Table 1). The remaining holes were employed to study alternative carbonate systems. The loaded cassettes were placed in a vacuum oven, heated to 240ºC for 1 hour, then cooled

to 130 °C and stored for 8-12 hours prior to loading. Prepared assemblies were stored at 130ºC in a vacuum oven for 1-2 hours prior to compression. During opening the vacuum oven was filled with dry air.

All experiments were performed as follows. The assemblies were compressed at room temperature to 6.0 MN in DIA press, or to 4.5 MN in wedge press, corresponding to pressure of 6.0 ± 0.5 GPa (Shatskiy et al., 2013c). Then the samples were heated to temperatures ranging from 900 to 1400 °C. The heating time ranged from 15 min to 32 h depending on temperature conditions. The temperature was maintained within 0.5 °C of the desired value using T. Katsura's software. The maximum temperature difference between samples did not exceed 20 °C (see Fig. 3 in Shatskiy et al. (2013c)). Experiments were terminated by cutting off the electrical power of heater, followed by slow decompression.

Since the Na_2CO_3-bearing samples are hygroscopic, a special care was taken to minimize the the duration of contact between sample and air. Recovered samples were mounted into an epoxy resin and polished under low-viscosity oil using 400-, 1000- and 1500-mesh sandpapers and 3-μm diamond paste. The sample surface was cleaned using an oil spray between each step of polishing. Finally we used petroleum benzene to remove oil after polishing immediately prior to coating and loading the sample into a scanning electron microscope.

Samples were studied using a Tescan MYRA 3 LMU scanning electron microscope (Tescan) coupled with an INCA Energy dispersive X-ray microanalysis system 450 equipped with the liquid nitrogen-free Large area EDS X-Max-80 Silicon Drift Detector (Oxford Instruments) at V.S. Sobolev IGM SB RAS (Novosibirsk, Russia). The EDS

116 spectra were collected by rastering the electron beam over a surface area available for the
117 analysis with linear dimensions from 10 to 300 μm at 20 kV accelerating voltage and 1
118 nA beam current. Counting times for spectra and X-ray elemental map collection were
119 20-30 seconds. No beam damage or change in measured composition with time was
120 observed. We also confirmed that the size of the analyzed region has no measurable
121 effect on the resulting data, as long as the area is significantly larger than the grain size.
122 The EDS spectra were optimized for the quantification using standard XPP procedure
123 included into the INCA Energy 450 software.

124 Finally we have checked the EDS calibration using post-experimental samples with
125 known compositions and a homogeneous texture synthesized below eutectic temperatures.
126 We found that deviation of Na/Fe ratio measured by EDS from the actual sample
127 composition did not exceed a confidence limit of our measurements (≤ 0.5 mol%).

128 The Raman measurements were performed using a Horiba J.Y. LabRAM HR800
129 Raman spectrometer equipped with an Olympus BX41 confocal microscope at IGM SB
130 RAS (Novosibirsk, Russia). Spectra were recorded at room temperature with the 514 nm
131 line of a CVI Melles Griot Ar-ion laser (~1 mW at the sample) and spectral resolution of
132 approximately 2 cm^{-1}. An Olympus 100 × 0.9 objective (100× magnification and a NA of
133 0.9) was used to focus the laser beam onto the sample and to collect the Raman signal.

134 The angle dispersive X-ray diffraction study of recovered samples was performed in
135 the Siberian Synchrotron and Terahertz Radiation Center. Measurements were curried out
136 at the 4th beamline of the VEPP-3 storage ring with 0.3685 Å wavelength and MAR345
137 image plate detector (Ancharov et al., 2001). The FIT2D program (Hammersley et al.,

1996) was used to integrate two-dimensional images to one-dimensional patterns; the WinXPOW program suite was employed for peak fitting and indexing.

3. Experimental results

Selected backscattered electron (BSE) images of sample cross-sections in the system Na_2CO_3-$(Fe_{0.87}Mn_{0.06}Mg_{0.07})CO_3$ are shown in Figure 1. The subsolidus samples are represented by homogeneous aggregates of carbonate phases, with grain size varying from several micrometers to several tens of micrometers (Fig. 1a-c). After annealing of mixtures with $X(Na_2CO_3) \leq 40$ mol% at 900 ºC for 32 h., the limited reagent (Na_2CO_3) was completely consumed to form $Na_2Fe(CO_3)_2$ (Fig. 1c, Table 1), while in the samples with $X(Na_2CO_3) \geq 60$ mol% relicts of siderite remains within $Na_2Fe(CO_3)_2$ grains (Fig. 1a, Table 1). In the same run and $X(Na_2CO_3) = 50$ mol%, the sample consists of $Na_2Fe(CO_3)_2$ and relicts of siderite and Na_2CO_3 solid solution (Fig. 1b, Table 1). At 1000 ºC after 20 hours, the limited reagents have been consumed almost completely (Fig. 1d), except the 50 mol% mixture, which contains appreciable amount of siderite (Fig. 1e, Table 1). Besides, the samples contain an intermediate compound, $Na_4Fe(CO_3)_3$, which appears at the $Na_2Fe(CO_3)_2$-Na_2CO_3 interfaces at $X(Na_2CO_3) = 70$ and 80 mol% (Fig. 1d,e) and within $Na_2Fe(CO_3)_2$ aggregate at $X(Na_2CO_3) = 60$-10 mol%. Considering the textural features and topology of the phase diagram, the $Na_4Fe(CO_3)_3$ compound is most probably metastable phase, which appears as an intermediate compound in following reactions:

$$4Na_2CO_3 + 2FeCO_3 \rightarrow Na_2CO_3 + Na_4Fe(CO_3)_3 + Na_2Fe(CO_3)_2 \rightarrow$$
$$2Na_2CO_3 + 2Na_2Fe(CO_3)_2;$$

$$3Na_2CO_3 + 3FeCO_3 \rightarrow Na_4Fe(CO_3)_3 + Na_2Fe(CO_3)_2 + FeCO_3 \rightarrow$$

161 $3Na_2Fe(CO_3)_2$;

162 $3Na_2CO_3 + 4FeCO_3 \rightarrow Na_4Fe(CO_3)_3 + Na_2Fe(CO_3)_2 + 2FeCO_3 \rightarrow$

163 $3Na_2Fe(CO_3)_2 + FeCO_3$.

164 The incipient melting has been established at 1000 °C at $X(Na_2CO_3)$ = 80 and 60
165 mol% (Fig. 1d,f, Table 1). At 80 mol% the resulting melt interfaces with the Na_2CO_3
166 solid solution (Fig. 1d), whereas at 60 mol% the melt contacts with the $Na_2Fe(CO_3)_2$
167 layer (Fig. 1f). In both cases the melt contains about 66 mol% Na_2CO_3 (Table 1). An
168 appearance of Na_2CO_3 solid solution layer at the HT side of the sample with $X(Na_2CO_3)$
169 = 70 mol% may be considered as a sign of melting (Fig. 1e). The melt could be
170 segregated at the HT side of the capsule above or beneath the cross-section of the sample.
171 No melting has been observed at $X(Na_2CO_3) \leq 50$ mol% (Fig. 1g). At 1100 ºC, the 60
172 mol% mixture underwent complete melting, while minor amounts of Na_2CO_3 and siderite
173 crystals were remained at the LT sides at $X(Na_2CO_3)$ = 70 and 50 mol%, respectively (Fig.
174 1h,i). The melt coexisting with Na_2CO_3 solid solution at $X(Na_2CO_3)$ = 70 and 80 mol%
175 contains about 69 mol% Na_2CO_3 and consists of dendritic aggregate of natrite and Fe-
176 eitelite. (Table 1). The siderite volume fraction increasing successively when $X(Na_2CO_3)$
177 changes from 50 to 10 mol% (Fig. 1i,j), while the Na_2CO_3 content in the melt remains
178 constant near 53 mol% (Table 1). The Na_2CO_3 content in the melt coexisting with
179 Na_2CO_3 solid solution increases from 74 to 86 mol%, when temperature increases from
180 1200 to 1300 °C (Table 1). The Na_2CO_3 content in the melt coexisting with siderite
181 decreases from 53 to 35 mol% with increasing temperature from 1200 to 1400 °C. The
182 melt quenched products consist of dendritic aggregate of Fe-eitelite and siderite.

Natural siderite used in the experiments contained minor Mn and Mg admixtures (6 mol% $MnCO_3$ and 7 mol% $MgCO_3$, respectively), which indicates that the studied system was pseudobinary. It can be suggested that these components do not affect the phase diagram significantly; however, minor modifications can be possible. Although the concentration of $MnCO_3$ in siderite remains nearly constant in all experiments, the $MgCO_3$ content is proportional to the degree of melting. It increases with temperature and/or $X(Na_2CO_3)$ (Table 1, 2). The consecutive increase of Mg number of siderite has to extend its stability to higher temperatures compared to the pure end member. On the other hand, the Mg admixture in the system could not affect the eutectic temperature, because Mg does not enter to the eutectic melt (Table 1).

The Mn/(Fe+Mn+Mg) ratio in $Na_2Fe(CO_3)_3$ is similar to siderite, typically 5-6 mol%, while the Mg/(Fe+Mn+Mg) ratio increases from 7 to 14 mol% with decreasing Na_2CO_3 content in the system at 900 °C. At 1000 ºC this compositional trend is not clear, probably due to presence of $Na_4Fe(CO_3)_3$. The latter phase is enriched in manganese, Mn/(Fe+Mn+Mg) = 9-10 mol%, and depleted in magnesium, Mg/(Fe+Mn+Mg) = 0-5 mol% (Table 1). In addition to carbonates the run products contain minor amounts of iron oxide, FeO and/or Fe_3O_4 (Table 1). The appearance of iron oxides in the subsolidus run products is most likely due to partial oxidation of siderite during drying of starting mixtures.

Selected Raman spectra of obtained carbonate phases are shown in Figure 2. The spectra from Na_2CO_3 solid solution (Fig. 2a) correspond to the γ-modification of Na_2CO_3, natrite (White, 1974). The spectrum of the new $Na_4Fe_{0.9}Mn_{0.1}(CO_3)_3$ compound shows three intense bands at 1092, 1084 and 1064 cm^{-1} assigned to the CO_3^{2-} ν_1 symmetric

206 stretching vibration. A single band at about 868 cm^{-1} can be assigned as an out-of-plane
207 bending motion (v_2) (White, 1974; Sharma and Simons, 1980). Broad and diffuse bands
208 near 1350 cm^{-1} and 1560 cm^{-1} may be ascribed to transverse optical (TO) and longitudinal
209 optical (LO) vibration modes, respectively, similarly to γ-Na_2CO_3 (Brooker and Bates,
210 1971). Two bands at 680 and 732 cm^{-1} are assigned to the v_4 in-plane deformation mode
211 of carbonate ion (White, 1974). The spectra also revealed low wavenumber bands at 74,
212 119, 161, 235, and 368 cm^{-1}, which may be assigned to the external vibration modes
213 between the cation and anion group (Fig. 2b).

214 The Raman spectra of $Na_2Fe_{0.85}Mn_{0.05}Mg_{0.10}(CO_3)_2$ recovered from experiments at
215 6 GPa and 900-1000 °C show a set of bands similar to the spectrum of $Na_2Mg(CO_3)_2$
216 eitelite, which has rhombohedral $R\bar{3}$ structure (Pabst, 1973; White, 1974; Shatskiy et al.,
217 2013a), but shifted to lower wavenumbers (Fig. 2c). The spectra have a single, strong
218 band at 1093 cm^{-1}, which can be attributed to the CO_3^{2-} v_1 symmetric stretching mode.
219 Weak bands at 180 and 247 cm^{-1} are due to lattice vibration. A very intense lattice mode
220 at 93 cm^{-1} may be due to the motion of the highly polarized Na ion (White, 1974). Two
221 bands at 702 and 730 cm^{-1} are assigned to the v_4 in-plane deformation mode of carbonate
222 ion (White, 1974). No intensity was observed in the frequency range 2900–4000 cm^{-1}
223 suggesting absence of hydration of studied carbonates.

224 The representative X-ray diffraction (XRD) patterns of samples recovered from run
225 ES354 conducted at 1000 °C and 6 GPa are shown in Fig. 3. The sample with $X(Na_2CO_3)$
226 = 50 mol% consists of Fe-eitelite (about 95 %) and minor amounts of siderite and
227 unknown phase (Fig. 3a). The sample with $X(Na_2CO_3)$ = 70 mol% contains Fe-eitelite,
228 natrite and new phase (Fig. 3b). Fe-eitelite has rhombohedral $R\bar{3}$ structure with cell

parameters a = 4.9712(16) Å, c = 16.569(4) Å, V = 354.61(22) Å^3 (Tabl. 2). For comparison, the cell dimensions of $Na_2Mg(CO_3)_2$ eitelite are a = 4.942(2) Å, c = 16.406 (7) Å (Pabst, 1973). The X-ray diffraction patterns of new $Na_4Fe(CO_3)_3$ compound were indexed assuming orthorhombic system (Fig. 3, Tabl. 3). Dimensions of the cell are a = 10.217(17) Å, b = 7.235(19) Å, c = 5.265 (4) Å, V = 389.10(11) Å^3.

Discussion

The Na_2CO_3-$FeCO_3$ phase diagram. Phase relations established in the system Na_2CO_3-$(Fe_{0.87}Mn_{0.06}Mg_{0.07})CO_3$ at 6 GPa are illustrated in Figure 4. The system has one intermediate compound: $Na_2Fe(CO_3)_2$, whose stoichiometry is similar to the double carbonates in the Na_2CO_3-$MgCO_3$ and K_2CO_3-$MgCO_3$ systems at 6 GPa (Shatskiy et al., 2013a; Shatskiy et al., 2013c). The $Na_2Fe(CO_3)_2$ compound has an upper stability limit of about 1050 °C, where it melts incongruently to siderite and liquid containing about 55 mol% Na_2CO_3. The Na_2CO_3-$Na_2Fe(CO_3)_2$ eutectic is established at 1000 ºC and 66 mol% Na_2CO_3. This eutectic temperature is about 200 °C lower than that established in the (K or Na)$_2CO_3$-(Ca or Mg)CO_3 binary systems at 6 GPa (Shatskiy et al., 2013a; Shatskiy et al., 2013c; Shatskiy et al., 2013d). Siderite remains as a subliquidus phase at 1400 ºC at $X(Na_2CO_3) \leq 30$ mol%. In contrast to the low-pressure data (Weidner, 1972), we did not observe thermal decomposition of siderite to iron oxide and CO_2. In contrast, we found that siderite melts incongruently above 1580 °C and 6 GPa to a carbonate-oxide liquid and CO_2 fluid phase (Shatskiy et al., 2014a). Similar melting reaction was reported for $CaCO_3$ at 0.1 GPa and 1300 °C (Wyllie, 1967).

The Na_2CO_3-$FeCO_3$-$MgCO_3$ phase diagram. The ternary Na_2CO_3-$FeCO_3$-$MgCO_3$ phase diagram can be constrained combining data from the present experiments with similar data along the Na_2CO_3-$MgCO_3$ and $FeCO_3$-$MgCO_3$ binary joins (Shatskiy et al., 2013a; Shatskiy et al., 2014a). The temperature of magnesite congruent melting (*Tm*) is inferred from the experimental data at 3 GPa, 1575 < *Tm* < 1595 °C, at 3.6 GPa, 1600 < *Tm* < 1620 °C, (Irving and Wyllie, 1975), at 8 GPa, 1900 < *Tm* < 2000 °C, and at 15 GPa, 1900 < *Tm* < 2000 °C (Katsura and Ito, 1990). The Na_2CO_3-$MgCO_3$ (Shatskiy et al., 2013a) and Na_2CO_3-$FeCO_3$ systems (Fig. 4) have similar topology with intermediate $Na_2(Fe,Mg)(CO_3)_2$ compound, which melts congruently at the Mg-rich side and incongruently at the Fe-rich side. The $MgCO_3$-$FeCO_3$ system appears to be a solid solution series (our unpublished data). We assumed continuous solid solution between $Na_2Fe(CO_3)_2$ and $Na_2Mg(CO_3)_2$ based on the following observations. (1) The Mg partitioning between coexisting phases causes formation of Mg-rich eitelite, $Na_2Fe_{0.81}Mn_{0.05}Mg_{0.14}(CO_3)_2$ (Table 1). (2) The $Na_2Fe_{0.3}Mn_{0.1}Mg_{0.6}(CO_3)_2$ solid solution has been reported in hydrothermalites of the Khibiny alkaline igneous complex, Kola Peninsula, Russia (Khomyakov et al., 1980). A general topology of the ternary diagram is shown in Figure 5. At $X(Na_2CO_3)$ > 50 mol%, melting in the ternary system is controlled by an cotectic, which temperature and composition gradually shift from 1200 ºC and Na# = 71 mol% to 1000 ºC and Na# = 66 mol% as $X(MgCO_3)$ = Mg/(Mg+Mn+Fe) decreases from 100 to 0 mol%. At $X(Na_2CO_3)$ < 50 mol%, melting in the ternary system is controlled by eutectic, at the Mg-rich side and by peritectic at the Fe-rich side. As $X(MgCO_3)$ decreases, the eutectic shifts from 1225 ºC and Na# = 48 mol% toward lower temperatures and Na# = 50 mol%, where it changes to peritectic, which shifts to 1050 ºC

and Na# = 55 mol%. The measurable amounts of $MgCO_3$ (up to 9 mol%) and $FeCO_3$ (up to 3 mol%) in Na_2CO_3 suggest an existence of the limited range of sodium carbonate solid solutions (Fig. 5).

Implication for incipient melting in the upper mantle. The presence of variable carbonates in mantle lithologies is apparent through the occurrence of calcite, dolomite, magnesite, siderite, eitelite [$Na_2Mg(CO_3)_2$], northupite [$Na_3Mg(CO_3)_2Cl$], nyerereite [$Na_2Ca(CO_3)_2$], and burkeite [$Na_6(CO_3)(SO_4)_2$] in mantle xenoliths and as inclusions in diamonds (Bulanova and Pavlova, 1987; Wang et al., 1996; Sobolev et al., 1997; Stachel et al., 1998; Stachel et al., 2000; Phillips et al., 2004; Zedgenizov et al., 2004; Kaminsky et al., 2009a; Korsakov et al., 2009; Bulanova et al., 2010; Golovin et al., 2012; Kaminsky et al., 2013; Sharygin et al., 2013). The carbonate composition is determined by the mantle lithology (peridotitic or eclogitic) and by *PT* conditions (Yaxley and Brey, 2004; Brey et al., 2008). Although CO_2 enters to the subduction zones mainly in the form of calcite in hydrothermally altered basalts (Alt and Teagle, 1999; Jarrard, 2003), carbonates exhumed from the mantle depths are often dolomitic in composition (Sobolev and Shatsky, 1990; Murakami et al., 2008). This is because calcite subjected to the *PT* conditions of eclogite facies as a part of basaltic oceanic crust reacts with garnet to form $(Ca,Mg,Fe)CO_3$ solid solutions accordingly to the reaction (Yaxley and Brey, 2004):

$$6CaCO_3(\text{calcite}) + (Mg,Fe)_3Al_2Si_3O_{12}(\text{garnet}) = 3(Ca,Mg,Fe)(CO_3)_2(\text{solid solutions}) + Ca_3Al_2Si_3O_{12}(\text{grossular}). \quad (3)$$

Extrapolation of the solidus of the carbonated eclogite EC1 determined by Yaxley and Brey (2004) to 6 GPa suggests the temperature of about 1340 °C. This value closely

296 matches the 1350 °C minimum melting temperature at 6 GPa for the $CaCO_3$-$MgCO_3$
297 binary reported by Buob et al. (2006).

298 Experiments in the model peridotite (CaO-MgO-Al_2O_3-SiO_2-CO_2, CMAS-CO_2)
299 systems showed that magnesite is stable subsolidus phase in ultramafic mantle. The
300 presence of magnesite depresses the solidus temperatures of mantle peridotites by more
301 than 300 °C (from 1750 to 1380 °C) at 6 GPa and yields magnesium dolomitic
302 carbonatite melt (Dalton and Presnall, 1998; Brey et al., 2008). The dominant melting
303 reaction at the solidus of magnesite-bearing lherzolite (Dasgupta and Hirschmann, 2007)
304 is:

305 $CaMgSi_2O_6(CPx) + 2MgCO_3(Mt) = CaMg(CO_3)_2(L) + Mg_2Si_2O_6(OPx)$.

306 However, experimental solidi of natural magnesite peridotite (1230 °C at 6 GPa
307 (Dasgupta and Hirschmann, 2006)) and natural eclogite + 5% CO_2 (1070 °C at 6 GPa
308 (Dasgupta et al., 2004)) are 120-280 °C lower than the melting minimum on the join
309 $CaCO_3$–$MgCO_3$. The difference most likely reflecting the fluxing effects of Na_2O and
310 FeO (Dasgupta and Hirschmann, 2007).

311 According to our data at 6 GPa the presence of Na_2CO_3 substantially decreases
312 temperature of incipient melting in the carbonated systems to 1225 °C for $MgCO_3$
313 (Shatskiy et al., 2013a), to 1200 °C for $CaCO_3$ (Shatskiy et al., 2013d), to 1100 °C for
314 $CaMg(CO_3)_2$ (our unpublished data), and to 1050 °C for $FeCO_3$ (this study). Although the
315 Na_2CO_3-$FeCO_3$ join shows coolest solidus, it is unlikely that $FeCO_3$ makes a significant
316 contribution to the lowering of solidus temperature of the Na_2CO_3-$FeCO_3$-$MgCO_3$-
317 $CaCO_3$ system and, therefore, solidus temperatures of carbonated peridotite and eclogite.

Summarizing above data we can conclude that: (i) adding of $FeCO_3$ would not change the Na_2CO_3-$MgCO_3$-$CaCO_3$ topology, because the topologies of Na_2CO_3-$MgCO_3$ and Na_2CO_3-$FeCO_3$ binaries and $MgCO_3$-$CaCO_3$ and $FeCO_3$-$CaCO_3$ binaries are essentially the same (Buob et al., 2006; Shatskiy et al., 2013a; Shatskiy et al., 2014a); (ii) since the Fe component forms continuous solid solutions with subliquidus phases: magnesite, dolomite, Mg-calcite and eitelite; the natural abundance of Fe cannot dramatically change solidus temperature in the Na_2CO_3-$MgCO_3$-$CaCO_3$ system. Therefore, the maximum contribution of $FeCO_3$ component into the lowering solidus temperatures of carbonated mantle could not exceed several tens °C.

Acknowledgements

We thank Oliver Tschauner for editorial handling and useful suggestions. We gratefully acknowledge anonymous reviewers for comments which help to improve the manuscript. This work was supported by the Russian Scientific Fund (proposal No. 14-17-00609) and performed under the project of the Ministry of education and science of Russian Federation (No. 14.B25.31.0032). The work was carried out involving the equipment belonging to the Siberian Synchrotron and Terahertz Radiation Center (Novosibirsk, Russia).

Figure captions

Fig. 1. Representative BSE images of sample cross-sections illustrating phase relations in the system Na_2CO_3-$(Fe_{0.87}Mn_{0.06}Mg_{0.07})CO_3$ at 6 GPa. Na_2ss = Na_2CO_3-siderite solid solution; Na_4Fe = $Na_4Fe(CO_3)_3$; Na_2Fe = $Na_2Fe(CO_3)_2$; Sd = siderite; L =

liquid. The high-temperature edge of the capsule is located at the upper side of each image. The white bar in each image is a scale 200 μm in length.

Fig. 2. Representative Raman spectra of natrite (a), $Na_4Fe_{0.9}Mn_{0.1}(CO_3)_3$ (b), $Na_2Fe_{0.85}Mn_{0.05}Mg_{0.01}(CO_3)_2$ (c) and siderite (d) from the samples synthesized in the system Na_2CO_3-$(Fe_{0.87}Mn_{0.06}Mg_{0.07})CO_3$ at 6 GPa and 1000 ^oC. The spectra were collected at ambient conditions.

Fig. 3. Angle-dispersive X-ray diffraction patterns of the samples recovered from the run ES354 at 1000 °C, 6 GPa and duration 20 h. (a) $X(Na_2CO_3)$ = 50 mol%. (b) $X(Na_2CO_3)$ = 70 mol%.

Fig. 4. The phase relations in the system Na_2CO_3-$(Fe_{0.87}Mn_{0.06}Mg_{0.07})CO_3$ at 6 GPa. Grey and open circles mark melt and Na_2ss compositions measured by EDS. Grey areas in the circles denote phases remaining in trace amount either due to kinetic problems or phases observed in the lower temperature side of partially molten samples. Na_2ss = Na_2CO_3-siderite solid solution; Na_2Fe = $Na_2Fe(CO_3)_2$; Sd = siderite; L = liquid.

Fig. 5. Isobaric *T*-*X* diagram for the ternary system Na_2CO_3-$MgCO_3$-$Fe_{0.96}Mn_{0.06}CO_3$ at 6 GPa. The temperature of siderite incongruent melting is from (Shatskiy et al., 2014b). The temperature of magnesite congruent melting (*Tm*) is inferred from the experimental data (Irving and Wyllie, 1975; Katsura and Ito, 1990).

References cited

Alt, J.C., and Teagle, A.H. (1999) The uptake of carbon duringalteration of ocean crust. Geochimica et Cosmochimica Acta, 63(10), 1527-1535.

Ancharov, A.I., Manakov, A.Y., Mezentsev, N.A., Tolochko, B.P., Sheromov, M.A., and Tsukanov, V.M. (2001) New station at the 4th beamline of the VEPP-3 storage ring. Nuclear Instruments and Methods in Physics Research Section A: Accelerators, Spectrometers, Detectors and Associated Equipment, 470(1), 80-83.

Boulard, E., Gloter, A., Corgne, A., Antonangeli, D., Auzende, A.L., Perrillat, J.P., Guyot, F., and Fiquet, G. (2011) New host for carbon in the deep Earth. Proceedings of the National Academy of Sciences of the United States of America, 108(13), 5184-5187.

Boulard, E., Menguy, N., Auzende, A.L., Benzerara, K., Bureau, H., Antonangeli, D., Corgne, A., Morard, G., Siebert, J., Perrillat, J.P., Guyot, F., and Fiquet, G. (2012) Experimental investigation of the stability of Fe-rich carbonates in the lower mantle. Journal of Geophysical Research-Solid Earth, 117, B02208.

Brey, G.P., Bulatov, V.K., and Girnis, A.V. (2011) Melting of K-rich carbonated peridotite at 6-10 GPa and the stability of K-phases in the upper mantle. Chemical Geology, 281(3-4), 333-342.

Brey, G.P., Bulatov, V.K., Girnis, A.V., and Lahaye, Y. (2008) Experimental melting of carbonated peridotite at 6-10 GPa. Journal of Petrology, 49(4), 797-821.

Brooker, M.H., and Bates, J.B. (1971) Raman and Infrared Spectral Studies of Anhydrous Li_2CO_3 and Na_2CO_3. Journal of Chemical Physics, 54(11), 4788-&.

Bulanova, G.P., and Pavlova, L.P. (1987) Magnesite peridotite assemblage in diamond from the Mir pipe. Doklady Akademii Nauk SSSR, 295(6), 1452-1456.

Bulanova, G.P., Walter, M.J., Smith, C.B., Kohn, S.C., Armstrong, L.S., Blundy, J., and Gobbo, L. (2010) Mineral inclusions in sublithospheric diamonds from Collier 4 kimberlite pipe, Juina, Brazil: subducted protoliths, carbonated melts and primary kimberlite magmatism. Contributions to Mineralogy and Petrology, 160(4), 489-510.

Buob, A., Luth, R.W., Schmidt, M.W., and Ulmer, P. (2006) Experiments on $CaCO_3$-$MgCO_3$ solid solutions at high pressure and temperature. American Mineralogist, 91(2-3), 435-440.

Cooper, A.F., Gittins, J., and Tuttle, O.F. (1975) The system Na_2CO_3-K_2CO_3-$CaCO_3$ at 1 kilobar and its significance in carbonatite petrogenesis. American Journal of Science, 275(5), 534-560.

Dalton, J.A., and Presnall, D.C. (1998) The continuum of primary carbonatitic-kimberlitic melt compositions in equilibrium with lherzolite: Data from the system CaO-MgO-Al_2O_3-SiO_2-CO_2 at 6 GPa. Journal of Petrology, 39(11-12), 1953-1964.

Dasgupta, R., and Hirschmann, M.M. (2006) Melting in the Earth's deep upper mantle caused by carbon dioxide. Nature, 440(7084), 659-662.

Dasgupta, R., and Hirschmann, M.M. (2007) Effect of variable carbonate concentration on the solidus of mantle peridotite. American Mineralogist, 92(2-3), 370-379.

Dasgupta, R., and Hirschmann, M.M. (2010) The deep carbon cycle and melting in Earth's interior. Earth and Planetary Science Letters, 298(1-2), 1-13.

Dasgupta, R., Hirschmann, M.M., and Withers, A.C. (2004) Deep global cycling of carbon constrained by the solidus of anhydrous, carbonated eclogite under upper mantle conditions. Earth and Planetary Science Letters, 227(1-2), 73-85.

Eitel, W., and Skaliks, W. (1929) Some double carbonates of alkali and earth alkali. Zeitschrift Fur Anorganische Und Allgemeine Chemie, 183(3), 263-286.

Franzolin, E., Schmidt, M.W., and Poli, S. (2011) Ternary Ca–Fe–Mg carbonates: subsolidus phase relations at 3.5 GPa and a thermodynamic solid solution model

including order/disorder. Contributions to Mineralogy and Petrology, 161(2), 213-227.

Genge, M.J., Price, G.D., and Jones, A.P. (1995) Molecular-dynamics simulations of CaCO3 melts to mantle pressures and temperatures - implications for carbonatite magmas. Earth and Planetary Science Letters, 131(3-4), 225-238.

Golovin, A.V., Sharygin, I.S., Korsakov, A.V., and Pokhilenko, N.P. (2012) Can parental kimberlite melts be alkali-carbonate liquids: Results of investigation of composition melt inclusions in the mantle xenoliths from kimberlites. 10th International Kimberlite Conference, p. 10IKC-91, Bangalore, India.

Grassi, D., and Schmidt, M.W. (2011) The melting of carbonated pelites from 70 to 700 km depth. Journal of Petrology, 52(4), 765-789.

Guillot, B., and Sator, N. (2011) Carbon dioxide in silicate melts: A molecular dynamics simulation study. Geochimica Et Cosmochimica Acta, 75(7), 1829-1857.

Hammersley, A.P., Svensson, S.O., Hanfland, M., Fitch, A.N., and Hausermann, D. (1996) Two-dimensional detector software: from real detector to idealised image or two-theta scan. International Journal of High Pressure Research, 14(4-6), 235-248.

Hammouda, T., and Laporte, D. (2000) Ultrafast mantle impregnation by carbonatite melts. Geology, 28(3), 283-285.

Hunter, R.H., and McKenzie, D. (1989) The equilibrium geometry of carbonate melts in rocks of mantle composition. Earth and Planetary Science Letters, 92(3-4), 347-356.

Irving, A.J., and Wyllie, P.J. (1975) Subsolidus and melting relationships for calcite, magnesite and the join $CaCO_3$-$MgCO_3$ to 36 kb. Geochimica et Cosmochimica Acta, 39(1), 35-53.

Jarrard, R.D. (2003) Subduction fluxes of water, carbon dioxide, chlorine, and potassium. Geochemistry Geophysics Geosystems, 4(5), 8905.

Kaminsky, F., Wirth, R., Matsyuk, S., Schreiber, A., and Thomas, R. (2009a) Nyerereite and nahcolite inclusions in diamond: evidence for lower-mantle carbonatitic magmas. Mineralogical Magazine, 73(5), 797-816.

Kaminsky, F.V., Khachatryan, G.K., Andreazza, P., Araujo, D., and Griffin, W.L. (2009b) Super-deep diamonds from kimberlites in the Juina area, Mato Grosso State, Brazil. Lithos, 112, 833-842.

Kaminsky, F.V., Wirth, R., and Schreiber, A. (2013) Carbonatitic inclusions in deep mantle diamond from Juina, Brazil: new minerals in the carbonate-halide association. The Canadian Mineralogist, 51(5), 669-688.

Katsura, T., and Ito, E. (1990) Melting and subsolidus relations in the $MgSiO_3$–$MgCO_3$ system at high pressures: implications to evolution of the Earth's atmosphere. Earth and Planetary Science Letters, 99(1-2), 110–117.

Khomyakov, A.P., Sandomirskaya, S.M., and Malinovskii, Y.A. (1980) Iron Eitelite, $Na_2(Mg,Fe)(CO_3)_2$: A New Mineral Variety. Doklady Akademii Nauk SSSR, 255(5), 1256-1259.

Klein-BenDavid, O., Logvinova, A.M., Schrauder, M., Spetius, Z.V., Weiss, Y., Hauri, E.H., Kaminsky, F.V., Sobolev, N.V., and Navon, O. (2009) High-Mg carbonatitic microinclusions in some Yakutian diamonds - a new type of diamond-forming fluid. Lithos, 112(S2), 648-659.

Korsakov, A.V., Golovin, A.V., De Gussem, K., Sharygin, I.S., and Vandenabeele, P. (2009) First finding of burkeite in melt inclusions in olivine from sheared lherzolite xenoliths. Spectrochimica Acta Part A: Molecular and Biomolecular Spectroscopy, 73(3), 424-427.

Lavina, B., Dera, P., Downs, R.T., Yang, W.G., Sinogeikin, S., Meng, Y., Shen, G.Y., and Schiferl, D. (2010) Structure of siderite $FeCO_3$ to 56 GPa and hysteresis of its spin-pairing transition. Physical Review B, 82(6), 064110.

Lecuyer, C., and Ricard, Y. (1999) Long-term fluxes and budget of ferric iron: implication for the redox states of the Earth's mantle and atmosphere. Earth and Planetary Science Letters, 165(2), 197-211.

Litasov, K.D., Shatskiy, A., Gavryushkin, P.N., Sharygin, I.S., Dorogokupets, P.I., Dymshits, A.M., Ohtani, E., Higo, Y., and Funakoshi, K. (2013a) *P-V-T* equation of state of siderite to 33 GPa and 1673 K. Physics of the Earth and Planetary Interiors, 224, 83-87.

Litasov, K.D., Shatskiy, A., and Ohtani, E. (2013b) Earth's Mantle Melting in the Presence of C–O–H–Bearing Fluid. In S. Karato, Ed. Physics and chemistry of the deep Earth, DOI: 10.1002/9781118529492.ch2, p. 38-65. John Wiley & Sons, Ltd. .

Litasov, K.D., Shatskiy, A., Ohtani, E., and Yaxley, G.M. (2013c) The solidus of alkaline carbonatite in the deep mantle. Geology, 41(1), 79-82.

Minarik, W.G., and Watson, E.B. (1995) Interconnectivity of carbonate melt at low melt fraction. Earth and Planetary Science Letters, 133(3-4), 423-437.

Murakami, T., Wallis, S., Enami, M., and Kagi, H. (2008) Forearc diamond from Japan. Geology, 36(3), 219-222.

Nagai, T., Ishido, T., Seto, Y., Nishio-Hamane, D., Sata, N., and Fujino, K. (2010) Pressure-induced spin transition in $FeCO_3$-siderite studied by X-ray diffraction measurements. Journal of Physics: Conference Series, 215, 012002.

Navon, O. (1991) High internal pressure in diamond fluid inclusions determined by infrared absorption. Nature, 353(6346), 746-748.

Ono, S., Kikegawa, T., and Ohishi, Y. (2007) High-pressure transition of $CaCO_3$. American Mineralogist, 92(7), 1246-1249.

Pabst, A. (1973) The crystallography and structure of eitelite, $Na_2Mg(CO_3)_2$. American Mineralogist, 58(3-4), 211-217.

Phillips, D., Harris, J.W., and Viljoen, K.S. (2004) Mineral chemistry and thermobarometry of inclusions from De Beers Pool diamonds, Kimberley, South Africa. Lithos, 77(1), 155-179.

Santillán, J., and Williams, Q. (2004) A high-pressure infrared and X-ray study of $FeCO_3$ and $MnCO_3$: comparison with $CaMg(CO_3)_2$-dolomite. Physics of the Earth and Planetary Interiors, 143-144, 291-304.

Schrauder, M., and Navon, O. (1994) Hydrous and carbonatitic mantle fluids in fibrous diamonds from Jwaneng, Botswana. Geochimica Et Cosmochimica Acta, 58(2), 761-771.

Sharma, S.K., and Simons, B. (1980) Raman study of K_2CO_3-$MgCO_3$ glasses. Carnegie Inst Washington Yearb, 79, 322-326.

Sharygin, I.S., Golovin, A.V., Korsakov, A.V., and Pokhilenko, N.P. (2013) Eitelite in sheared peridotite xenoliths from Udachnaya-East kimberlite pipe (Russia) – a new locality and host rock type. European Journal of Mineralogy, 25, 825-834.

Shatskiy, A., Borzdov, Y.M., Litasov, K.D., Kupriyanov, I.N., Ohtani, E., and Palyanov, Y.N. (2014a) Phase relations in the system $FeCO_3$-$CaCO_3$ at 6 GPa and 900-1700 °C and its relation to the system $CaCO_3$-$FeCO_3$-$MgCO_3$. American Mineralogist, 99(4), 773-785.

Shatskiy, A., Gavryushkin, P.N., Sharygin, I.S., Litasov, K.D., Kupriyanov, I.N., Higo, Y., Borzdov, Y.M., Funakoshi, K., Palyanov, Y.N., and Ohtani, E. (2013a) Melting and subsolidus phase relations in the system Na_2CO_3-$MgCO_3$+-H_2O at 6 GPa and the stability of $Na_2Mg(CO_3)_2$ in the upper mantle. American Mineralogist, 98(11-12), 2172-2182.

Shatskiy, A., Katsura, T., Litasov, K.D., Shcherbakova, A.V., Borzdov, Y.M., Yamazaki, D., Yoneda, A., Ohtani, E., and Ito, E. (2011) High pressure generation using scaled-up Kawai-cell. Physics of the Earth and Planetary Interiors, 189(1-2), 92-108.

Shatskiy, A., Litasov, K.D., Borzdov, Y.M., Katsura, T., Yamazaki, D., and Ohtani, E. (2013b) Silicate diffusion in alkali-carbonatite and hydrous melts at 16.5 and 24 GPa: Implication for the melt transport by dissolution-precipitation in the transition zone and uppermost lower mantle. Physics of the Earth and Planetary Interiors, 225, 1-11.

Shatskiy, A., Litasov, K.D., Ohtani, E., Borzdov, Y.M., and Palyanov, Y.N. (2014b) The systems K_2CO_3-$FeCO_3$ and $MgCO_3$-$FeCO_3$ at 6 GPa and 900-1700 ^oC. European Journal of Mineralogy, Under review.

Shatskiy, A., Sharygin, I.S., Gavryushkin, P.N., Litasov, K.D., Borzdov, Y.M., Shcherbakova, A.V., Higo, Y., Funakoshi, K., Palyanov, Y.N., and Ohtani, E. (2013c) The system K_2CO_3-$MgCO_3$ at 6 GPa and 900-1450 ºC. American Mineralogist, 98(8-9), 1593-1603.

Shatskiy, A., Sharygin, I.S., Litasov, K.D., Borzdov, Y.M., Palyanov, Y.N., and Ohtani, E. (2013d) New experimental data on phase relations for the system Na_2CO_3-$CaCO_3$ at 6 GPa and 900-1400 ºC. American Mineralogist, 98(11-12), 2164-2171.

Sobolev, N.V., Kaminsky, F.V., Griffin, W.L., Yefimova, E.S., Win, T.T., Ryan, C.G., and Botkunov, A.I. (1997) Mineral inclusions in diamonds from the Sputnik kimberlite pipe, Yakutia. Lithos, 39(3-4), 135-157.

Sobolev, N.V., and Shatsky, V.S. (1990) Diamond inclusions in garnets from metamorphic rocks: a new environment for diamond formation. Nature, 343(6260), 742-746.

Stachel, T., Harris, J.W., and Brey, G.P. (1998) Rare and unusual mineral inclusions in diamonds from Mwadui, Tanzania. Contributions to Mineralogy and Petrology, 132(1), 34-47.

Stachel, T., Harris, J.W., Brey, G.P., and Joswig, W. (2000) Kankan diamonds (Guinea) II: lower mantle inclusion parageneses. Contributions to Mineralogy and Petrology, 140(1), 16-27.

Tomlinson, E.L., Jones, A.P., and Harris, J.W. (2006) Co-existing fluid and silicate inclusions in mantle diamond. Earth and Planetary Science Letters, 250(3-4), 581-595.

548 Wang, A., Pasteris, J.D., Meyer, H.O.A., and DeleDuboi, M.L. (1996) Magnesite-bearing
549 inclusion assemblage in natural diamond. Earth and Planetary Science Letters,
550 141(1-4), 293-306.
551 Weidner, J.R. (1972) Equilibria in the system Fe-C-O; Part I, Siderite-magnetite-carbon-
552 vapor equilibrium from 500 to 10,000 bars American Journal of Science, 272(8),
553 735-751.
554 Weiss, Y., Kessel, R., Griffin, W.L., Kiflawi, I., Klein-BenDavid, O., Bell, D.R., Harris,
555 J.W., and Navon, O. (2009) A new model for the evolution of diamond-forming
556 fluids: Evidence from microinclusion-bearing diamonds from Kankan, Guinea.
557 Lithos, 112(S2), 660-674.
558 White, W.B. (1974) The carbonate minerals. In V.C. Farmer, Ed. The Infrared Spectra of
559 the Minerals, Mineralogical Society Monograph, p. 227-284. Mineralogical
560 Society, London.
561 Wyllie, P.J. (1967) Phase equilibria in system CaO-CO_2-H_2O and related systems, with
562 Implications for crystal growth of calcite and apatite. Journal of the American
563 Ceramic Society, 50(1), 43-46.
564 Yaxley, G.M., and Brey, G.P. (2004) Phase relations of carbonate-bearing eclogite
565 assemblages from 2.5 to 5.5 GPa: implications for petrogenesis of carbonatites.
566 Contributions to Mineralogy and Petrology, 146(5), 606-619.
567 Yoshino, T., Laumonier, M., McIsaac, E., and Katsura, T. (2010) Electrical conductivity
568 of basaltic and carbonatite melt-bearing peridotites at high pressures: Implications
569 for melt distribution and melt fraction in the upper mantle. Earth and Planetary
570 Science Letters, 295(3-4), 593-602.
571 Zedgenizov, D.A., Kagi, H., Shatsky, V.S., and Sobolev, N.V. (2004) Carbonatitic melts
572 in cuboid diamonds from Udachnaya kimberlite pipe (Yakutia): evidence from
573 vibrational spectroscopy. Mineralogical Magazine, 68(1), 61-73.
574 Zedgenizov, D.A., Ragozin, A.L., Shatsky, V.S., Araujo, D., Griffin, W.L., and Kagi, H.
575 (2009) Mg and Fe-rich carbonate-silicate high-density fluids in cuboid diamonds
576 from the Internationalnaya kimberlite pipe (Yakutia). Lithos, 112(S2), 638-647.
577 Zedgenizov, D.A., Rege, S., Griffin, W.L., Kagi, H., and Shatsky, V.S. (2007)
578 Composition of trapped fluids in cuboid fibrous diamonds from the Udachnaya
579 kimberlite: LAM-ICPMS analysis. Chemical Geology, 240(1-2), 151-162.
580

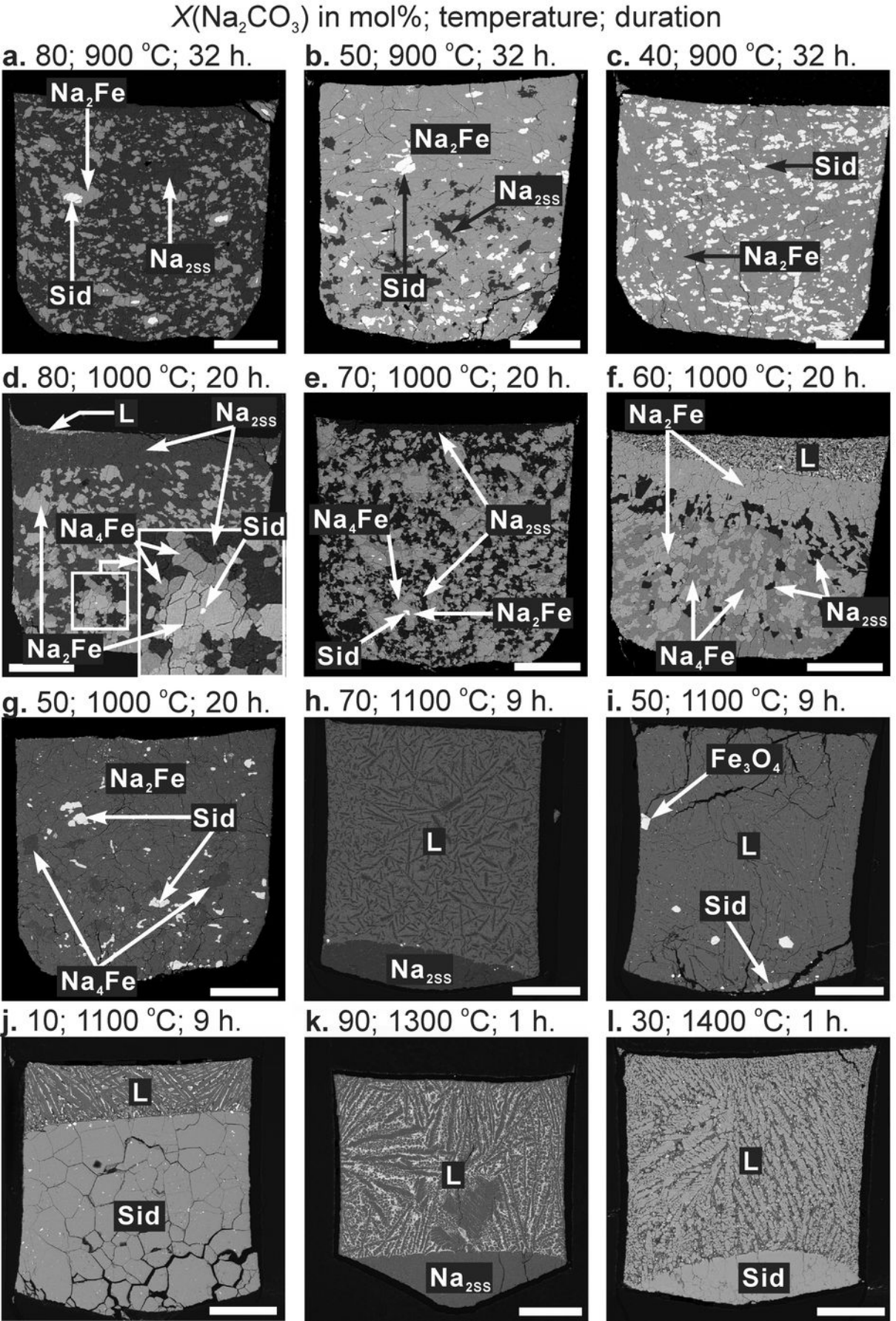
X(Na2CO3) in mol%; temperature; duration
a. 80; 900 °C; 32 h.
Na2Fe
Na2ss
Sid
b. 50; 900 °C; 32 h.
Na2Fe
Na2ss
Sid
c. 40; 900 °C; 32 h.
Sid
Na2Fe
d. 80; 1000 °C; 20 h.
L
Na2ss
Na4Fe
Sid
Na2Fe
e. 70; 1000 °C; 20 h.
Na4Fe
Na2ss
Na2Fe
Sid
f. 60; 1000 °C; 20 h.
Na2Fe
L
Na2ss
Na4Fe
g. 50; 1000 °C; 20 h.
Na2Fe
Sid
Na4Fe
h. 70; 1100 °C; 9 h.
L
Na2ss
i. 50; 1100 °C; 9 h.
Fe3O4
L
Sid
j. 10; 1100 °C; 9 h.
L
Sid
k. 90; 1300 °C; 1 h.
L
Na2ss
l. 30; 1400 °C; 1 h.
L
Sid

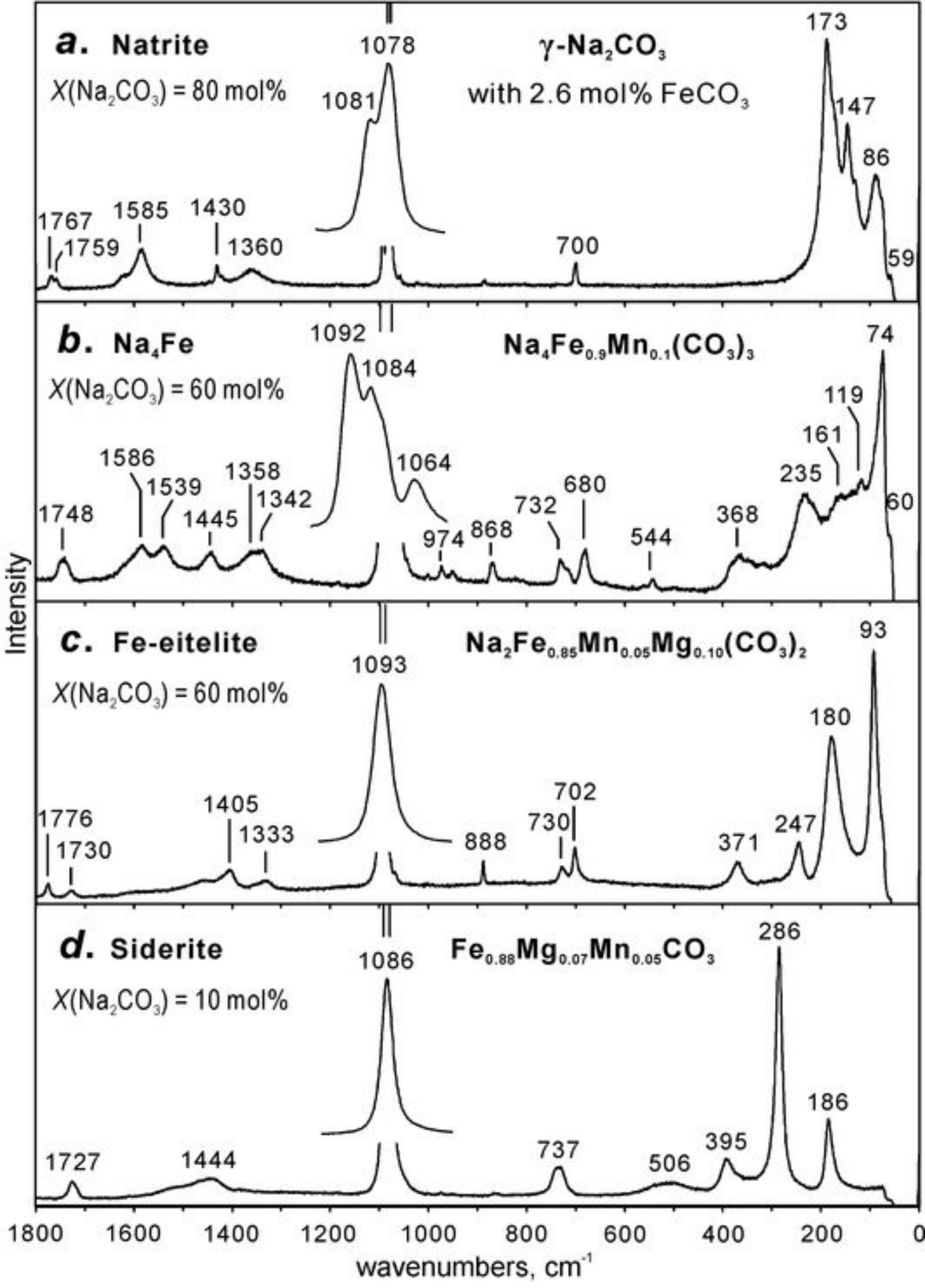
a. Natrite
X(Na2CO3) = 80 mol%
γ-Na2CO3
with 2.6 mol% FeCO3
1078
1081
1767
1759
1585
1430
1360
700
173
147
86
59
b. Na4Fe
X(Na2CO3) = 60 mol%
Na4Fe0.9Mn0.1(CO3)3
1092
1084
1064
1748
1586
1539
1445
1358
1342
974
868
732
680
544
368
235
161
119
74
60
c. Fe-eitelite
X(Na2CO3) = 60 mol%
Na2Fe0.85Mn0.05Mg0.10(CO3)2
1093
1776
1730
1405
1333
888
730
702
371
247
180
93
d. Siderite
X(Na2CO3) = 10 mol%
Fe0.88Mg0.07Mn0.05CO3
1086
1727
1444
737
506
395
286
186
Intensity
1800
1600
1400
1200
1000
800
600
400
200
0
wavenumbers, cm-1

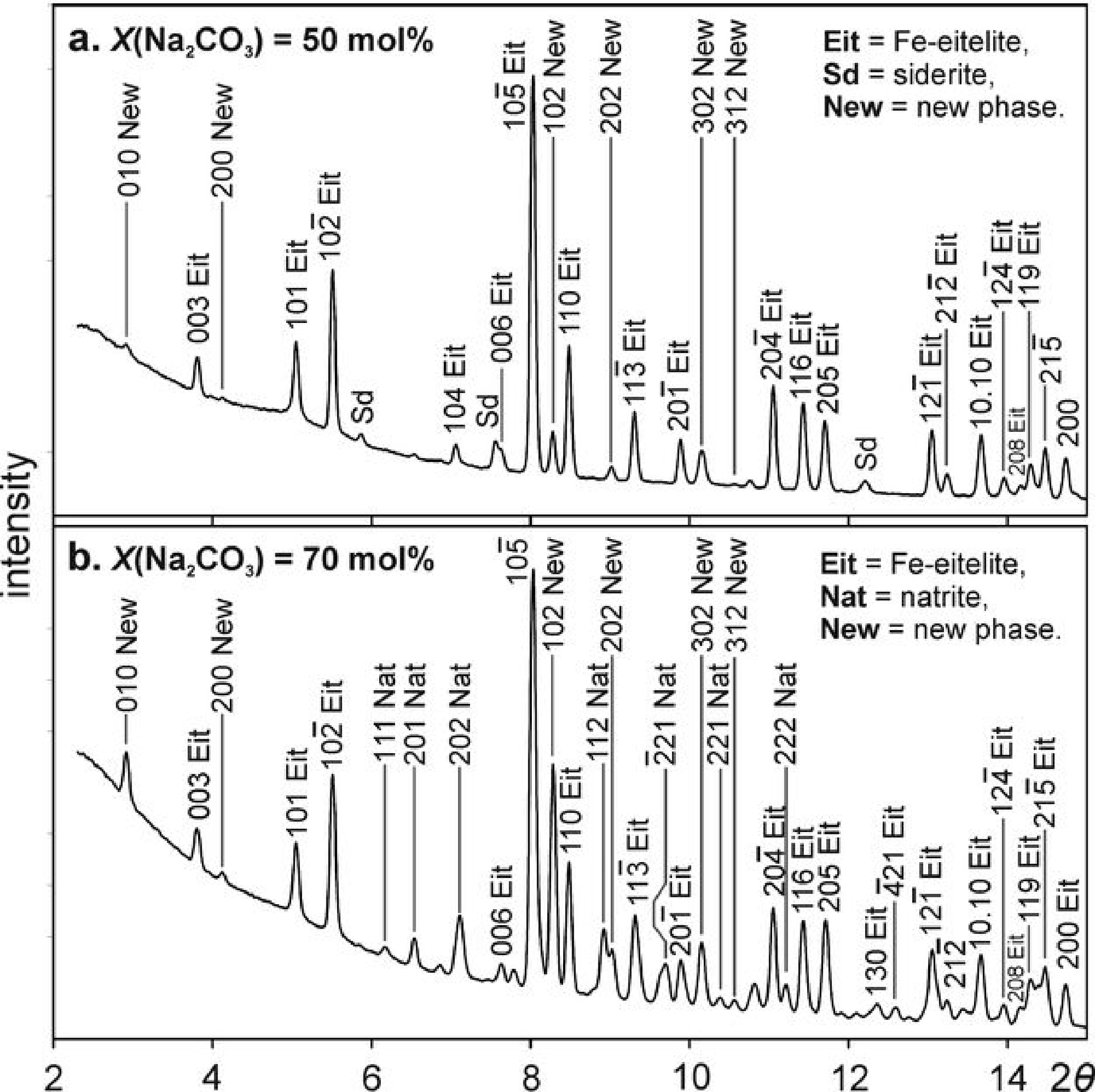
a. X(Na2CO3) = 50 mol%
Eit = Fe-eitelite,
Sd = siderite,
New = new phase.
010 New
200 New
003 Eit
101 Eit
10$\bar{2}$ Eit
Sd
104 Eit
Sd
006 Eit
10$\bar{5}$ Eit
102 New
110 Eit
202 New
11$\bar{3}$ Eit
20$\bar{1}$ Eit
302 New
312 New
20$\bar{4}$ Eit
116 Eit
205 Eit
Sd
12$\bar{1}$ Eit
21$\bar{2}$ Eit
10.10 Eit
12$\bar{4}$ Eit
208 Eit
119 Eit
21$\bar{5}$
200
b. X(Na2CO3) = 70 mol%
Eit = Fe-eitelite,
Nat = natrite,
New = new phase.
010 New
200 New
003 Eit
101 Eit
10$\bar{2}$ Eit
111 Nat
201 Nat
202 Nat
006 Eit
10$\bar{5}$
102 New
110 Eit
112 Nat
202 New
11$\bar{3}$ Eit
$\bar{2}$21 Nat
20$\bar{1}$ Eit
302 New
221 Nat
312 New
20$\bar{4}$ Eit
222 Nat
116 Eit
205 Eit
130 Eit
$\bar{4}$21 Eit
12$\bar{1}$ Eit
21$\bar{2}$
10.10 Eit
12$\bar{4}$ Eit
208 Eit
119 Eit
21$\bar{5}$ Eit
200 Eit
intensity
2
4
6
8
10
12
14
2θ

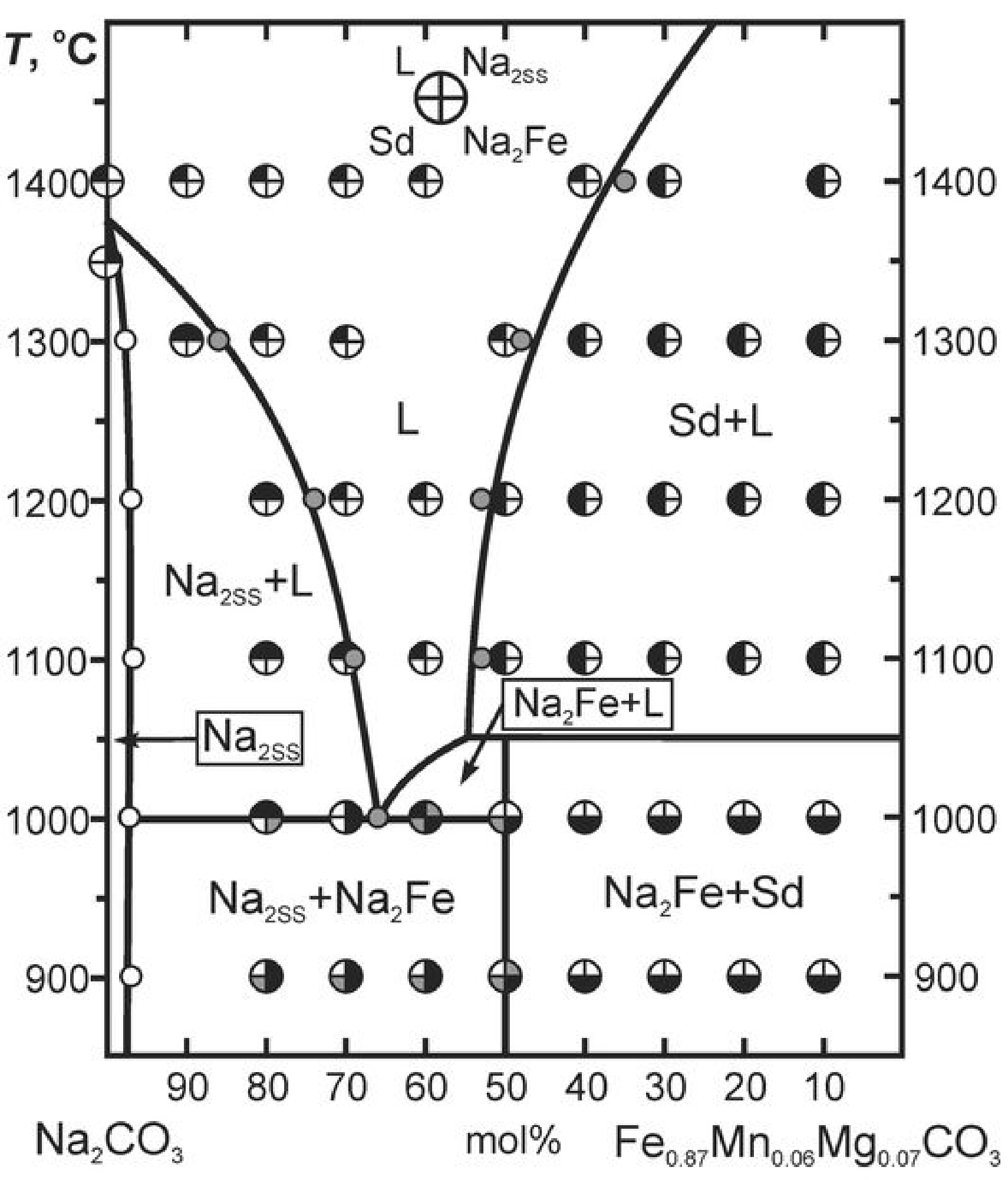
T, °C
L
Na2ss
Sd
Na2Fe
1400
1300
1200
1100
1000
900
L
Sd+L
Na2ss+L
Na2Fe+L
Na2ss
Na2ss+Na2Fe
Na2Fe+Sd
90
80
70
60
50
40
30
20
10
Na2CO3
mol%
Fe0.87Mn0.06Mg0.07CO3

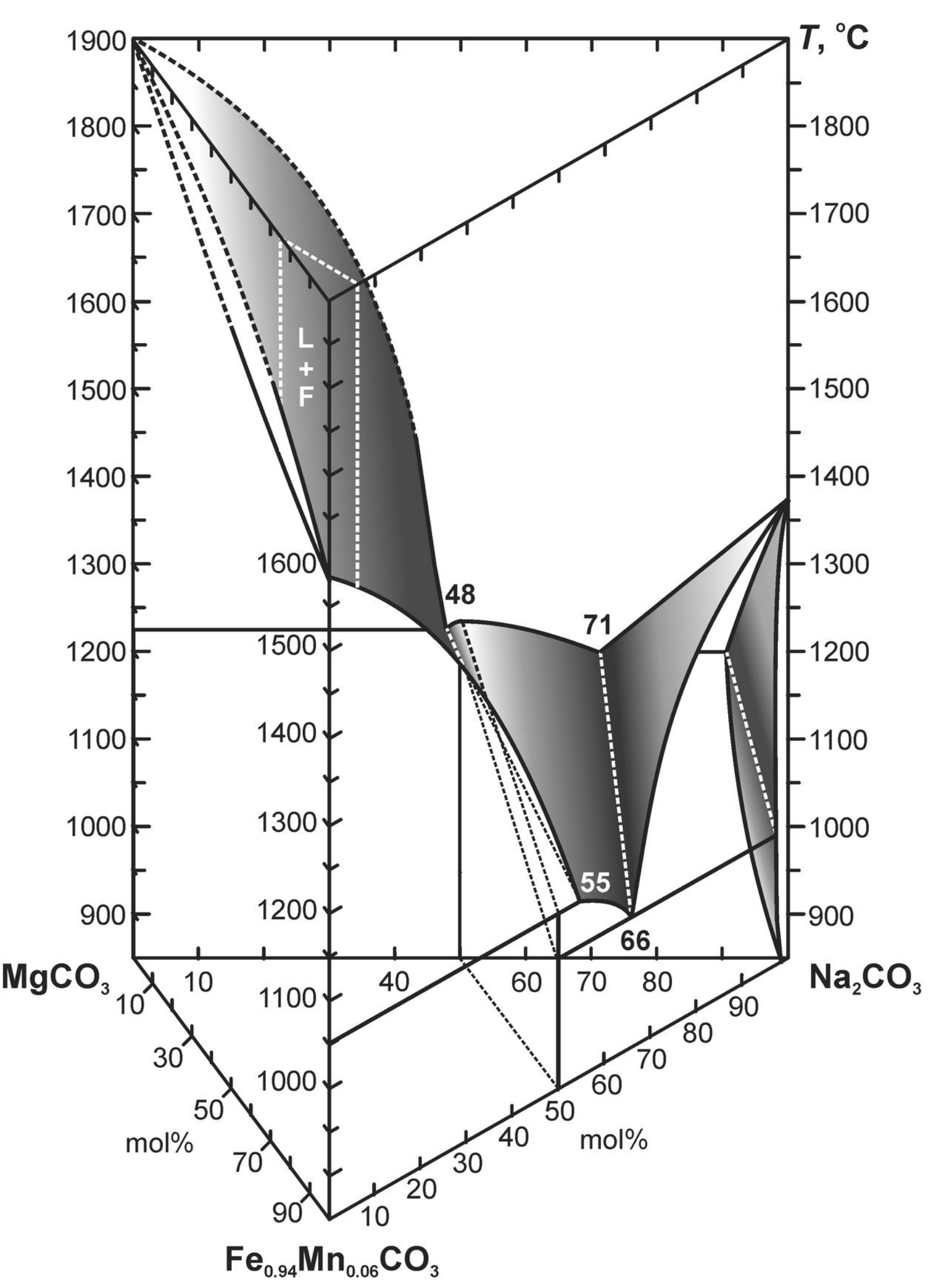
T, °C
1900
1800
1700
1600
1500
1400
1300
1200
1100
1000
900
L + F
48
71
55
66
MgCO3
Na2CO3
Fe0.94Mn0.06CO3
mol%
mol%
10
30
50
70
90
20
40
60
80

Table. 1. Compositions of the run products in the system Na_2CO_3-$(Fe_{0.87}Mn_{0.06}Mg_{0.07})CO_3$ at 6 GPa.

#, T, τ	X_{Na}	Phase	Compositions in wt%					Compositions in mol%			
			Na_2O	FeO	MnO	MgO	Total	Na_2#	Fe#	Mn#	Mg#
T2078, 1400°C, 15 min	90	L	46.3(2)	7.3(3)	0.5(0)	0.3(0)	54.4(5)	86.7(4)	88.0(2)	5.5(2)	6.5(0)
	80	L	47.1(2)	10.0(0)	0.5(0)	0.4(0)	57.9(2)	83.0(0)	89.4(1)	4.7(3)	5.9(2)
	70	L	40.6(3)	17.2(6)	1.1(0)	0.8(1)	59.7(1.0)	70.6(6)	87.7(2)	5.6(0)	6.7(2)
	60	FeO	n.d.	93.9(5)	0.7(1)	n.d.	94.8(5)	n.d.	99.3(1)	0.7(1)	n.d.
		L	35.0(2)	22.1(2)	1.3(1)	1.0(1)	59.5(1)	61.6(4)	87.6(1)	5.3(2)	7.0(4)
	40	L	25.1(1)	37.9(1)	2.4(1)	1.8(0)	67.2(1)	40.0(1)	87.0(2)	5.6(1)	7.4(1)
	30	Sd	n.d.	52.9(4)	3.1(1)	4.4(1)	60.3(5)	n.d.	82.9(2)	4.8(1)	12.3(3)
		L	21.8(1.0)	41.5(1)	2.6(1)	1.6(2)	67.5(1.4)	34.9(8)	88.4(9)	5.5(2)	6.1(7)
	10	Sd	n.d.	52.6(4)	3.3(1)	3.4(1)	59.3(4)	n.d.	84.8(3)	5.5(2)	9.7(1)
		L	22.5	41.6	2.7	1.7	68.5	35.5	87.8	5.7	6.6
ES357, 1300°C, 1 h	90	Na_2	51.7(7)	1.5(2)	n.d.	n.d.	53.2(5)	97.7(3)	100.0(0)	n.d.	n.d.
		L	46.4(3)	7.7(4)	0.5(0)	n.d.	54.6(1)	86.8(7)	94.0(2)	6.0(2)	n.d.
	80	L	45.7	10.8	0.5	0.4	57.4	81.5	89.5	4.3	6.2
	70	L	41.7(2)	16.3(1)	1.0(0)	0.8(1)	59.8(2)	72.1(1)	87.2(8)	5.2(2)	7.6(6)
	60	FeO	n.d.	95.8(4)	0.7(1)	n.d.	96.5(5)	n.d.	99.3(1)	0.7(1)	n.d.
		L	36.3	21.7	1.4	1.1	60.5	62.7	86.8	5.6	7.6
	50	FeO	n.d.	96.2(5)	0.6(0)	n.d.	96.8(5)	n.d.	99.4(0)	0.6(0)	n.d.
		L	29.1	32.1	2.1	1.4	64.5	47.9	87.6	5.7	6.7
	30	Sd	n.d.	52.6(3)	3.0(1)	4.0(2)	59.3(3)	n.d.	83.8(5)	4.8(1)	11.4(4)
		L	29.4(5)	33.6(3)	2.1(1)	1.3(1)	66.3(7)	47.4(3)	88.6(1)	5.5(3)	5.9(3)
	20	Sd	n.d.	53.9(2)	3.1(2)	3.3(1)	60.2(2)	n.d.	85.7(2)	5.2(3)	9.1(1)
		L	30.8(3)	33.1(3)	2.3(0)	0.9(1)	67.1(5)	49.1(1)	89.3(4)	6.3(0)	4.3(4)
	10	Sd	n.d.	53.5(3)	3.4(1)	2.8(2)	59.6(2)	n.d.	86.5(4)	5.5(1)	8.0(4)
		L	28.7(4)	33.1(1)	2.4(2)	0.8(1)	64.9(0)	47.4(6)	89.6(6)	6.4(4)	3.9(2)
ES356, 1200°C, 5 h	80	Na_2	51.5(3)	1.9(0)	n.d.	n.d.	53.4(3)	96.9(0)	100.0(0)	n.d.	n.d.
		L	42.6	14.9	0.9	0.6	59.1	74.4	87.9	5.6	6.5
	70	L	41.1	17.0	1.0	0.7	59.9	71.1	87.9	5.4	6.8
	60	FeO	n.d.	96.9	0.6	n.d.	97.5	n.d.	99.4	0.6	n.d.
		L	34.4(1.4)	22.5(1.1)	1.5(2)	1.3(1)	59.6(0)	60.3(2.2)	85.8(5)	5.7(5)	8.5(0)
	40	Sd	n.d.	53.2(1)	2.9(0)	4.2(2)	60.3(2)	n.d.	83.7(5)	4.6(1)	11.6(4)
		FeO	n.d.	96.4	0.6	n.d.	97.0	n.d.	99.4	0.6	n.d.
		L	30.7(3)	28.6(0)	1.9(0)	1.2(1)	62.4(2)	52.1(3)	87.5(2)	6.0(0)	6.5(2)
	30	Sd	n.d.	53.7(5)	3.2(1)	3.2(1)	60.1(3)	n.d.	85.7(6)	5.1(3)	9.2(4)
		FeO	n.d.	95.0	0.6	n.d.	95.6	n.d.	99.4	0.6	n.d.
		L	29.1(2)	27.3(0)	2.2(0)	1.0(1)	59.6(1)	51.8(3)	87.1(5)	7.2(1)	5.8(6)
	20	Sd	n.d.	54.0(2)	3.2(1)	3.1(1)	60.3(2)	n.d.	86.0(3)	5.2(1)	8.7(3)
		L	31.7(9)	28.7(2)	2.0(1)	0.8(1)	63.1(8)	53.4(9)	89.3(5)	6.3(2)	4.4(3)
	10	Sd	n.d.	53.8(5)	3.3(1)	2.8(2)	59.8(4)	n.d.	86.7(5)	5.3(1)	8.0(5)
		L	31.8(4)	26.0(4)	1.9(0)	0.6(0)	60.3(0)	56.0(5)	89.7(5)	6.7(2)	3.5(2)
T2077, 1100°C, 9 h	80	Na_2	51.5(4)	2.5(1)	n.d.	n.d.	54.1(4)	95.8(2)	100.0(0)	n.d.	n.d.
		L	40.8(1)	16.4(3)	1.0(0)	1.0(1)	58.9(3)	71.5(5)	87.1(4)	5.2(1)	7.7(3)
	70	Na_2	51.5(7)	2.6(3)	n.d.	n.d.	54.3(6)	95.6(3)	100.0(0)	n.d.	n.d.
		L	40.8	18.2	1.1	n.d.	54.3(6)	69.6	87.9	5.4	6.7
	60	FeO	n.d.	96.6	0.6	n.d.	97.2	n.d.	99.4	0.6	n.d.
		L	35.0	22.0	1.4	1.1	59.5	61.5	86.9	5.5	7.6
	50	Sd	n.d.	52.7(3)	2.8(1)	5.0(1)	60.5(1)	n.d.	81.7(4)	4.3(2)	13.9(2)
		Fe_3O_4	n.d.	91.5	n.d.	n.d.	91.5	n.d.	100.0(0)	n.d.	n.d.
		L	30.4(2)	25.8(3)	1.7(0)	1.3(2)	59.1(3)	54.2(1)	86.8(8)	5.8(1)	7.5(1.0)
	40	Sd	n.d.	53.9(6)	3.1(1)	3.7(3)	60.7(5)	n.d.	84.7(7)	4.9(2)	10.4(7)
		Fe_3O_4	n.d.	91.6	n.d.	n.d.	91.6	n.d.	100.0(0)	n.d.	n.d.

		L	28.9(7)	27.1(4)	1.9(0)	1.0(0)	58.8(1.2)	52.1(3)	88.1(1)	6.2(0)	5.7(2)
	30	Sd	n.d.	54.3(8)	3.1(1)	3.2(1)	60.6(8)	n.d.	86.0(3)	5.0(1)	8.9(2)
		Fe_3O_4	n.d.	92.7	n.d.	n.d.	92.7	n.d.	100.0(0)	n.d.	n.d.
		L	29.1(2)	26.8(2)	1.8(0)	0.7(1)	58.3(1)	53.1(5)	90.0(4)	6.0(0)	4.0(5)
	20	Sd	n.d.	54.1(3)	3.3(1)	2.9(1)	60.3(1)	n.d.	87.3(4)	5.5(1)	7.2(4)
		L	29.1	27.3	1.9	0.7	59.1	52.5(1)	89.4	6.3	4.3
	10	Sd	n.d.	54.3(9)	3.4(1)	2.5(1)	60.2(9)	n.d.	87.3(4)	5.5(1)	7.2(4)
		L	27.8(1)	26.1(1)	1.9(2)	0.7(1)	56.4(1)	52.5(1)	89.6(1)	6.4(5)	4.0(4)
ES354, 1000°C, 20 h	80	Na_2	51.4(6)	1.6(1)	n.d.	n.d.	52.9(7)	97.4(2)	100.0(0)	n.d.	n.d.
		Na_4Fe	36.3	18.2	1.7	0.4	56.6	67.1	88.2	8.5	3.3
		Na_2Fe	29.0(2)	27.9(2)	1.4(1)	1.6(1)	59.8(4)	51.1(2)	86.9(6)	4.3(2)	8.8(6)
		L	34.2(5)	20.3(3)	1.4(1)	n.d.	55.9(7)	64.7(1)	93.5(5)	6.5(5)	n.d.
	70	Na_2	51.9(6)	1.6(1)	n.d.	n.d.	53.5(5)	97.5(1)	100.0(0)	n.d.	n.d.
		Na_4Fe	36.4(8)	17.6(8)	1.7(1)	0.1(3)	55.8(5)	68.3(1.8)	90.0(2.3)	8.7(3)	1.2(2.1)
		Na_2Fe	28.4(2)	27.8(4)	1.4(1)	1.5(1)	59.0(5)	50.9(1)	87.2(6)	4.5(3)	8.3(5)
		Sd	n.d.	52.9(7)	3.4(3)	2.6(9)	59.0(6)	n.d.	86.8(2.7)	5.6(3)	7.6(2.4)
	60	Na_2	51.4(6)	1.6(1)	n.d.	n.d.	52.9(7)	96.8(3)	100.0(0)	n.d.	n.d.
		Na_4Fe	37.7(4)	18.2(2)	1.8(1)	n.d.	57.7(4)	68.6(3)	90.9(5)	9.1(5)	n.d.
		Na_2Fe	28.7(2)	27.4(2)	1.5(1)	1.9(1)	59.4(4)	50.8(2)	85.2(4)	4.6(3)	10.3(6)
		L	36.0(1)	19.8(1)	1.2(0)	n.d.	57.0(2)	66.5(1)	94.2(0)	5.8(0)	n.d.
	50	Na_4Fe	36.8(6)	17.1(1)	1.9(1)	n.d.	55.8(7)	69.1(2)	89.9(4)	10.1(4)	n.d.
		Na_2Fe	27.9(2)	27.6(5)	1.6(1)	1.4(1)	58.5(7)	50.5(4)	87.1(6)	5.1(3)	7.8(7)
		Sd	n.d.	53.6(8)	3.3(2)	1.9(4)	58.7(2)	n.d.	89.0(1.6)	5.5(3)	5.5(1.3)
	40	Na_2Fe	28.4(3)	27.4(3)	1.7(1)	1.5(1)	59.0(6)	50.9(1)	86.1(2)	5.3(2)	8.6(4)
		Sd	n.d.	53.0(5)	3.5(3)	2.3(5)	58.7(4)	n.d.	87.4(1.7)	5.8(4)	6.8(1.3)
	30	Na_2Fe	28.8(4)	27.1(6)	1.8(1)	1.8(2)	59.5(9)	51.0(6)	84.2(7)	5.6(3)	10.2(9)
		Sd	n.d.	54.5(2)	3.3(1)	2.0(2)	59.9(5)	n.d.	88.9(7)	5.4(3)	5.7(6)
		Fe_3O_4	n.d.	92.0	n.d.	n.d.	92.0	n.d.	100.0(0)	n.d.	n.d.
	20	Na_2Fe	29.0(2)	26.7(2)	1.7(1)	2.2(1)	59.6(2)	51.0(3)	82.6(4)	5.3(2)	12.1(5)
		Sd	n.d.	53.5(3)	3.4(1)	2.4(3)	59.3(1)	n.d.	87.4(8)	5.6(2)	7.0(8)
	10	Na_4Fe	36.9(6)	15.6(2)	1.7(1)	0.5(0)	54.6(7)	70.2(3)	85.6(2)	9.4(5)	5.0(3)
		Na_2Fe	28.8	28.3	1.9	1.3	60.3	50.6	87.1	5.8	7.0
		Sd	n.d.	53.7(7)	3.3(1)	2.5(1)	59.5(9)	n.d.	87.4(1)	5.4(1)	7.2(1)
T2076, 900°C, 32 h	80	Na_2	51.3(6)	1.3(1)	n.d.	n.d.	52.6(7)	97.8(2)	100.0(0)	n.d.	n.d.
		Na_2Fe	29.2(3)	28.3(3)	1.7(1)	1.4(2)	60.6(6)	51.0(1)	87.0(8)	5.3(1)	7.7(9)
		Sd	n.d.	54.2(3)	3.5(1)	2.3(2)	60.0(4)	n.d.	87.6(7)	5.7(2)	6.6(6)
	70	Na_2	52.0(1.5)	1.3(1)	n.d.	n.d.	53.3(1.5)	97.8(2)	100.0(0)	n.d.	n.d.
		Na_2Fe	28.4(5)	28.0(2)	1.7(1)	1.3(1)	59.4(7)	50.7(4)	87.2(4)	5.4(2)	7.4(5)
		Sd	n.d.	54.4(5)	3.4(2)	1.7(4)	59.5(1)	n.d.	89.3(1.4)	5.7(2)	4.9(1.2)
	60	Na_2	52.3(2)	2.0(1)	n.d.	n.d.	54.2(2)	96.8(2)	100.0(0)	n.d.	n.d.
		Na_2Fe	28.8(1)	28.5(0)	1.7(1)	1.3(0)	60.2(1)	50.7(1)	87.7(1)	5.4(2)	6.9(3)
		Sd	n.d.	55.1(3)	3.5(2)	1.9(1)	60.6(2)	n.d.	88.8(1)	5.8(3)	5.5(1)
	50	Na_2	51.4(1)	1.5(1)	n.d.	n.d.	52.9(1)	97.5(2)	100.0(0)	n.d.	n.d.
		Na_2Fe	28.4(5)	28.1(2)	1.8(1)	1.4(1)	59.7(6)	50.4(4)	86.8(5)	5.6(2)	7.6(6)
		Sd	n.d.	52.2(2.0)	3.5(1)	1.9(1)	57.6(2.1)	n.d.	88.3(2)	6.1(3)	5.6(1)
	40	Na_2Fe	28.5(2)	27.8(2)	1.8(0)	1.4(1)	59.5(4)	50.8(2)	86.7(3)	5.6(1)	7.7(3)
		Sd	n.d.	55.0(9)	3.2(2)	1.8(1)	60.0(8)	n.d.	89.5(4)	5.3(2)	5.2(4)
	30	Na_2Fe	28.7(1)	27.7(1)	1.8(0)	1.6(3)	59.7(1)	50.4(1)	84.7(1)	5.5(1)	9.7(0)
		Sd	n.d.	54.3(8)	3.2(4)	2.0(1)	59.6(4)	n.d.	88.8(9)	5.4(8)	5.9(2)
	20	Na_2Fe	29.0(5)	26.8(7)	1.7(1)	2.2(1)	59.6(1.0)	50.9(7)	82.5(3)	5.2(1)	12.3(2)
		Sd	n.d.	54.6(1.0)	3.5(2)	2.0(3)	60.0(9)	n.d.	88.5(8)	5.8(3)	5.8(1)
	10	Na_2Fe	29.0(5)	26.9(5)	1.8(0)	2.6 (1)	60.3(1.0)	50.2(3)	80.6(0)	5.4(1)	14.0(0)
		Sd	n.d.	53.5(5)	3.4(2)	2.5(1)	59.3(5)	n.d.	87.3(5)	5.5(3)	7.2(3)

Notes: # = run number; τ = run duration; X_{Na}= Na_2CO_3 content in the system; Na_2# = Na_2CO_3 content in the run products; Fe# = Fe/(Fe+Mn+Mg); Mn# = Mn/(Fe+Mn+Mg); Mg# = Mg/(Fe+Mn+Mg); Na_2 = Na_2CO_3;

L = liquid; Sd = siderite; Na_2Fe = $Na_2Fe(CO_3)_2$; Na_4Fe = $Na_4Fe(CO_3)_3$. Standard deviations are given in parentheses, where the number of measurement is more than one.

Table 2. Interplanar spacings (d values) for $Na_2Fe_{0.87}Mn_{0.05}Mg_{0.8}(CO_3)_2$ eitelite synthesized at 6 GPa and 1000 °C (run ES354, $X(Na_2CO_3)$ = 50 mol%).

d	2θ	Int	*hkl*
5.544265	3.8089	8.68	003
4.181242	5.0512	18.52	101
3.831111	5.5132	40.7	012
2.991021	7.0634	5.41	104
2.767682	7.6342	4.63	006
2.630894	8.0318	100	015
2.490466	8.4855	32.4	110
2.270456	9.3095	17.2	113
2.137369	9.8905	10.77	021
2.075914	10.1841	2.16	107
1.912842	11.0549	25.34	024
1.849718	11.4334	21.4	116
1.80688	11.7054	17.48	205
1.621283	13.0509	16.24	211
1.59806	13.2414	5.51	122
1.54816	13.6702	15.18	1010
1.51624	13.9594	4.39	214
1.494857	14.1601	2.47	208
1.480616	14.297	7.69	119
1.462323	14.4768	11.86	125
1.436614	14.7373	9.83	300

Table 3. Interplanar spacings (d values) for $Na_4Fe_{0.9}Mn_{0.1}(CO_3)_3$ synthesized at 6 GPa and 1000 °C (run ES354, $X(Na_2CO_3)$ = 70 mol%).

d	2θ	Int	hkl
7.23847	2.9172	20	010
5.113432	4.1299	4	200
2.550317	8.2860	100	102
2.340075	9.0319	18	202
2.081418	10.1571	27	302
2.000422	10.5695	4	312